Climatology of Tropopause Folds over a European Arctic Station - ESRANGE

T. Narayana Rao*, J. Arvelius, and S. Kirkwood

Swedish Institute of Space Physics, BOX. 812, Kiruna- 981 28, Sweden
* Presently at National Atmospheric Research Laboratory, Gadanki – 517 112, India

Submission of the manuscript: 26 November 2007
Submission of the revised version: 07 March 2008

Abstract:

Eleven years (September 1996 - August 2007) of continuous measurements of three dimensional wind and backscattered signal strength observed with ESrange RADar (ESRAD) have been utilized to study the annual and interannual variation of tropopause folds over an Arctic station. Two typical tropopause fold events (one is associated with a streamer type of system and the other with a cut-off low) are selected and are characterized with the help of synoptic charts and potential vorticity (PV) analysis. Typical characteristics of radar parameters during the passage of folds are identified, such as the sudden rise in the tropopause altitude, high reflectivity layer sloping downward from the tropopause beneath the jet stream and intensification of the jet stream. These characteristics are utilized to discern the tropopause fold in the radar data. The climatology of tropopause folds exhibits a pronounced annual cycle with a large number of folds in winter and fewer in summer. The annual cycle of folds is more or less similar in all the years, however, significant interannual variation is observed with winter periods exhibiting maximum interannual variability. The climatology of folds and its annual cycle are compared and contrasted with similar climatological studies available in the literature. The differences in the climatologies are discussed in light of differences in the algorithms and the spatial variability of fold frequency.

1. Introduction:

At the extratropical tropopause, the exchange between the stratosphere and troposphere mainly occurs in tropopause folds [Danielsen, 1968; Shapiro, 1980; Keyser and Shapiro, 1986; WMO, 1986], cut-off lows [Price and Vaughan, 1993; Ancellet et al. 1994] and streamer-type systems [Appenzeller and Davies, 1992; Appenzeller et al., 1996]. In the literature, the contribution of these processes to the total stratosphere troposphere exchange (STE) is discussed controversially (refer the review article on STE by Holton et al., 1995). Traditionally tropopause folds are believed to be the major agents for STE. Sprenger et al. [2003], however, argued that the tropopause folds account only for 10-30% of all STE events in the extratropics and other processes like breakup of stratospheric streamers and erosion of cut-off lows are equally important for STE. In a recent study, they have shown the importance of PV streamers and cut-off lows for STE (Wernli and Sprenger, 2007; Sprenger et al., 2007) Among all STE processes, the structure, evolution, dissipation and climatology of cut-off lows are extensively studied [Price and Vaughan, 1992; Price and Vaughan, 1993; Ancellet et al., 1994; Ebel et al., 1996; Kentarchos and Davies, 1998; Fuenzalida et al., 2005; Nieto et al., 2005; Wernli and Sprenger, 2007]. These studies clearly show a geographical preference for their formation and also significant seasonal variation. A peak in summer in the annual cycle of cut-off lows over Europe in the northern hemisphere is found, while a summer minimum is found in South American and African sectors in the southern hemisphere. Cut-off lows promote exchange by vigorous convective mixing as well as through shear instabilities near jet streams. Streamers, which can be seen clearly in Meteosat water vapour images and on isentropic potential vorticity (PV) charts near the tropopause

region, are unstable to dynamical instabilities and eventually roll up into small vortices [Appenzeller and Davies, 1992; Appenzeller et al., 1996; Martius et al., 2007].

Dynamic processes leading to tropopause folding, as a result of cross frontal secondary circulation associated with jet streams in upper level troughs and cut-off lows, are well documented through extensive studies and measurements of folds. They include theoretical studies [Hoskins and Bretherton, 1972], in situ aircraft measurements [Danielsen, 1968; Shapiro, 1980], radar/lidar remote sensing techniques [Browell et al., 1987; Ancellet et al. 1994; Vaughan et al., 2001; Nastrom et al., 1989; Bertin et al., 2001; Rao et al., 2003; Rao and Kirkwood, 2005], satellite measurements [Wimmers and Moody, 2004] and meso-scale and synoptic-scale models [Ebel et al., 1991; Lamarque and Hess 1994]. These studies addressed various issues related to the tropopause folds, such as characteristics of folds, identification of folds from observational and model data sets, their role in instigating severe weather events, exchange of constituents occurring through the fold boundaries, etc.

However, some ambiguity remained in the seasonality of tropopause folds in the extratropics. Using PV and Q-vector divergence maxima as a criterion, Ebel et al. [1996] and Elbern et al. [1998] studied the global climatology of folds. They found that the number of folds is significantly smaller in summer than in other seasons. Contrary to the above result, Van Haver et al. [1996] and Beekmann et al. [1997] found a rather flat frequency distribution of folds at two mid-latitude European stations. They detected the folds in vertical ozonesonde profiles as ozone rich, dry, stable layers located in an upper level front. In fact, they observed a slight increase in fold frequency in summer, though it is not statistically significant at 2σ level. A similar analysis (but, using PV criteria instead

of stability criteria) making use of ozonesoundings at four European stations show a maximum fold occurrence in March and a minimum in April to June [Blonsky and Speth, 1998]. Rao et al. [2003] found no correlation between ozone mixing ratio and PV in the middle Arctic troposphere in the summer, whereas, a fair correlation is seen in other seasons. From these correlations, they speculated the seasonality of tropopause folds with a summer minimum. Sprenger et al. [2003] employed a purely geometric tropopause fold definition to examine the climatological aspects of STE. They also found that deep folds occurred predominantly in mid latitudes during winter. The apparent contradictions in the annual cycle of folds with different methods indicate that knowledge of the climatology of folds in the extratropics is still unclear and needs to be pursued further. It forms the central objective of the present investigation.

Further, studies of the climatology of folds at selected locations are confined to European mid latitude stations. The present article describes a method to identify the tropopause folds from VHF radar (ESrange RADar-ESRAD) measurements, and uses it to study the seasonal cycle and interannual variability of tropopause folds over an arctic station. The data used for the present study is described in Section 2. A description of the method for identifying the tropopause fold in ESRAD data is given in Section 3. Also included in the section 3 are the annual and interannual variations of fold occurrence. The pros and cons of the radar method against methods based on chemical and dynamical tracers are discussed in Section 4. The results are summarized in Section 5, which also contains a discussion of the fold statistics in light of other climatologies.

2. Data description:

ESRAD, a VHF radar located at Esrange (67°.53′ N, 21°.06′ E) near Kiruna in northern Sweden, has the ability to monitor winds and turbulence continuously in the troposphere and lower stratosphere. Useful returns are also obtained from the summer mesosphere to study Polar Mesosphere Summer Echoes (so called, PMSE). The radar operates at a frequency of 52 MHz and has a peak transmitted power of 72 kW. The antenna array consists of 12 x 12 (18 x 16 after April 2004), five-element yagis spaced at a distance of 0.7λ from each other, where λ is the radar wavelength. The two-way half-power-width of the main lobe is about 6 ° (4° after April 2004). ESRAD has 6 separate receivers to sample the return signal from the atmosphere, which will allow post-detection beam-steering and full spectral analysis of the returned signal. A complete description of the radar can be found in Chilson et al. [1999]. For the present study, data collected during September 1996-August 2007 are used. Due to technical problems, the radar data are not available during summer 1999. Except for this major data gap, other data gaps are very small in duration (less than about 4 days) as well as in number. The typical vertical resolution of the data is 300 m in the troposphere and lower stratosphere (150 m in May-December 2003 and after March 2005). The radar operates continuously cycling between modes optimized for troposphere, stratosphere, or mesosphere and (occasionally) meteor winds. Because of this, the time resolution varies from 1 min to about 10 min. Before 2002, most of the radar time during late spring to summer was devoted to modes optimized for PMSE. However, in other seasons the typical time resolution for tropospheric measurements is about 1 min.

In the present analysis, ECMWF analysis products with T106 resolution (1.125° x 1.125°) are utilized. The data prior (after) to 1 February 2006 are available at 60 (91) model levels for every 6 hours. The spectral data are interpolated and converted to regular grid intervals on pressure and theta surfaces using routines available at Norwegian Institute for Air Research (NILU). The radar and ECMWF analysis products have been supplemented by routine radiosoundings launched from Luleå (65.55° N, 22.13° E) and Bodo (67.25° N, 14.39° E). The radiosonde measurements (pressure, temperature, humidity, wind speed and direction) are available as a function of height at 00 and 12 UT.

3. Methodology and results:

Radars operating at VHF band, such as ESRAD, obtain backscatter from refractive index fluctuations, with scale lengths of the order of half the radar wavelength (Bragg condition). The radar reflectivity is proportional to the mean generalized refractive index gradient, M (m^{-1}), and is given [Ottersten, 1969] by

$$M = - 77.6 \times 10^{-6}(p/T)(d \ln \theta/dz) \{1 + 15500q/T[1 - (d \ln q/dz)/(2d \ln \theta/dz)]\} \quad (1)$$

where p is the pressure (hPa), T is the temperature (K), θ is the potential temperature (K) and q is the specific humidity (g/g). The specific humidity variations (second and third terms) play a major role in the lower and middle troposphere, whereas the radar reflectivity is proportional to the static stability (first term) in the upper troposphere and stratosphere (refer Hooper et al., 2004 and Luce et al., 2007 for more details on the relation between M and static stability). The dependence of radar reflectivity on static stability in dry and weakly humid regions has been effectively utilized by Gage and

Green [1979] to detect the altitude of the tropopause. Rottger [1979] used the same concept to describe the passage of a frontal system. A more detailed analysis of frontal zone and tropopause structures using a VHF radar and radiosondes has been given by Larsen and Rottger [1985] and Nastrom et al. [1989]. Recent observations by VHF radars for detecting tropopause folds, made use of the aspect sensitive property of VHF radars [Caccia and Cammas, 1998; Campistron et al., 1999; Caccia et al., 2000; Bertin et al., 2001], which depends on the stability of the atmosphere.

Hooper and Arvelius [2000] presented a radar tropopause detection algorithm (the altitude at which the vertical gradient of the echo power, evaluated over 1800 m, has its maximum value) using ESRAD data and found a good correspondence with the static stability tropopause. Their results clearly demonstrate the capability of ESRAD to observe highly stable regions, such as the tropopause and frontal structure. In the present analysis, the high stability regions have been detected from radar vertical reflectivity enhancements to build the climatology of the tropopause folds using ESRAD observations. The frontal zone is discerned from 3870 1-day time-height-intensity plots obtained from 11 years of ESRAD observations. Characteristics of tropopause folds from the radar point of view have been studied below during the passage of a streamer and a cutoff low over the radar location. Two cases were selected for a detailed study and are shown below.

3.1 Case study 1:

The passage of a streamer and associated tropopause fold observed on 16-17 January 2003 is described in this section with the help of synoptic charts, radiosonde and

radar measurements. The horizontal wind and PV (1 PV = 10^{-6} m^2 s^{-1} K kg^{-1}) maps are obtained from ECMWF analysis. Figure 1 shows the horizontal velocity field on the 300 hPa surface (left panel) along with PV on 310 K surface (right panel), observed during 16-17 January 2003, respectively. The synoptic situation on 16 January 2003 at 12 UT is dominated by an upper level pronounced ridge and an intensifying trough with an intense jet streak (with wind speeds in excess of 45 ms^{-1}) approaching the radar location from southwest. This intense upper level trough is associated with a relatively broad positive PV anomaly which narrows as it extends southwestward as a streamer. This elongated PV filament extending from the polar reservoir (east of Sweden) to southwest of Spain across Central Europe, rolls up into a small vortex. The streamer, however, advected over the radar location during this period. During the passage of this streamer, an intense tropopause fold is observed with ESRAD.

A typical example of an upper-air frontal zone as seen by ESRAD is shown in Figure 2. It includes the time-height section of signal-to-noise ratio, SNR (dB), zonal (ms^{-1}) and meridional (ms^{-1}) velocities and spectral width (ms^{-1}) observed with the ESRAD on 17 January 2003. The SNR is high in the lower troposphere as a result of humidity and temperature variations associated with strong turbulence and decreases with height up to the tropopause. A clear enhancement of SNR seen at around 8 km from 00 to 03 UT marks the height of the tropopause [Gage and Green, 1979; Hooper and Arvelius, 2000]. After 03 UT, the layer of enhanced SNR splits into two with one layer sloping downward from the tropopause and penetrating into the lower troposphere. The other layer, representing the tropopause, rises sharply by around 2 km and appears at around 10 km after 05 UT. The sloping enhanced SNR layer, corresponding to the frontal zone, is in

fact, not a single layer but a band of layers of high reflectivity separated by few kilometers. These layers appear as laminae in vertical soundings of chemical constituent fields, such as ozone [Danielsen et al., 1991; Reid and Vaughan, 1991]. Rao and Kirkwood [2005] observed good correspondence between the frontal zone and ozone enhancement in the ozone profile.

In the time-height section of velocity and spectral width plots (figures 2b-2d), the white area indicates the lack of useful data (SNR is less than 0 dB). It is clearly apparent from the figure that strong easterlies prevail throughout the day in the upper troposphere and lower stratosphere with wind speeds exceeding 50 ms^{-1}. The zonal velocity increased significantly by nearly a factor of 2 from 16 January 2007 at 12 UT (not shown in the figure) to 17 January at 06 UT (figure 2b). A strong enhancement in the vertical shear of horizontal wind is also observed along the frontal zone (sloping structure). The meridional velocities depict a trough structure with a reversal in the meridional wind direction from south to north during the observational period. Relatively larger spectral width values are seen along the frontal zone. All these features portray a classical example of a tropopause fold structure as described by Danielsen [1968], Shapiro [1980] and Rao and Kirkwood [2005].

Several other meteorological parameters have been examined to corroborate the passage of the jet stream and the front and also to find the magnitude of the jet. Note that, ESRAD may not always provide wind measurements in the upper troposphere due to the weak backscatter it gets from that region (white gaps shown in the figure 2). Therefore the required wind information is obtained from radiosonde measurements, albeit with poor temporal resolution. Routine radiosonde measurements close to the radar location

(Luleå and Bodo) have been utilized for this purpose. Note that, radiosonde measurements are included in the present context only to confirm the existence of a jet stream, rapid changes in wind speed/direction, and dry layer. Otherwise, the present analysis is independent of radiosonde measurements and identifies tropopause folds entirely from ESRAD data. Although the horizontal separation between ESRANGE and Bodo is larger, the radiosonde measurements from Bodo are included here; because Bodo lies west of the radar location. During the westerly wind period (which is predominant during winter), the balloon drifts toward the radar location. The overhead measurements made by the radar are therefore better compared to the balloon measurements of Bodo.

Vertical profiles of wind speed, wind direction and relative humidity observed by radiosondes at Luleå and Bodo during 16-17 January 2003 are shown in Figure 3. Similar wind patterns are observed at both locations. At around 12 UT on 16 Jan. 2003, the winds are generally weak (with speeds mostly confined to less than 30 ms^{-1}) in the troposphere and lower stratosphere, but intensified with time and attained maximum velocities, exceeding 60 ms^{-1}, in the upper troposphere. A change in the wind direction between 12 UT on 16 Jan 2003 and 00/12 UT on 17 Jan 2003 in the lower troposphere is clearly evident from the figure (middle panel) at Bodo, however, such a clear change in wind direction with time is not seen at Luleå. At both locations, no significant change in wind direction is observed in the middle-upper troposphere with winds remaining predominantly eastward throughout the observational period. The relative humidity profiles obtained at both Bodo and Luleå show the presence of a dry layer with RH < 10% at around 3 km on 17 Jan 2003 at 00 UT. Earlier studies using satellites, radiosoundings and trajectory-based simulations show large gradients in humidity in the

vicinity of the intrusions (in particular, along the frontal zone), with very dry air within the intrusions (RH < 20%) and very moist air ahead of the intrusions [Kiladis, 1998; Waugh, 2005, Rao and Kirkwood, 2005]. The vertical profile of humidity across the frontal zone, thus, shows a dry layer just below the moderately moist layer in the vicinity of the fold as shown in figure 3. Note that, high humidity over a dry layer in a humidity profile doesn't always mean a tropopause fold given the variability of humidity spatially and vertically. But, RH and wind measurements by radiosonde coupled with radar measurements confirm the existence of a fold.

3.2 Case study 2:

Tropopause folding which occurred beneath a closed circulation induced by a positive PV anomaly is discussed in this section. The synoptic feature that dominated during 30-31 July 2005 is a cut-off low system centered over northern Scandinavia with horizontal wind speeds in excess of 40 ms^{-1} at the 300 hPa level (figure 4). The positive PV anomalies can be seen on the 310 K surface as a blob of high PV within this closed circulation. The strongest PV anomaly, observed northwest of Scandinavia on 30 July 2005 at 18 UT, drifted eastward close to the radar location by 31 July 2005, 12 UT. This high PV is accompanied by an upper level jet with a jet streak lying close to the radar location. These conditions are ideal for the tropopause to fold from north of the jet steak sloping down towards the south beneath the jet.

Time-height sections of ESRAD parameters observed on 31 July 2005 (during the passage of the tropopause fold) are shown in figure 5. The general features of radar parameters are largely similar to those seen in case study 1. For example, sudden change

in the tropopause height, sloping frontal zone, intensification of horizontal wind, presence of strong turbulence along the frontal zone, etc. are seen in this event too. However, the change in the tropopause height during the upper air frontal passage is greater in this case (nearly 3-4 km against 2 km in case study 1). Similarly, laminae structures (the high reflectivity layers) are much more clear and significant in this case. However, the winds are generally weaker than that in case study 1. The radiosonde measurements at Bodo and Luleå also show some differences in vertical wind profiles (figure 6). There is a distinct intensification of the upper level jet observed within 12 hours at Bodo, from ~20 ms^{-1} on 30 July 2005 at 12 to ~45 ms^{-1} on 31 July 2005 at 00 UT. Such an intensification of the jet stream is absent over Luleå where upper level winds remain mostly at 30 ms^{-1}. As also is evident from figure 4, the cut-off low and the jet streak were located mostly north of Luleå during the observational period. However, the fold, sloping down from north to south, might have reached Luleå as is evident from the humidity profiles.

3.3 Climatology of tropopause folds:

The typical radar features seen in the case studies (and also in numerous case studies reported in the literature) are summarized here and are used to identify tropopause folds. One clear signature that is seen in all tropopause fold events is the sudden change in the tropopause altitude. Indeed, using this feature alone Nastrom et al. [1989] identified tropopause folds with the Flatland VHF radar. They have noted a clear association of tropopause altitude change with some upper air synoptic feature, such as front, trough, jet stream, etc. Several earlier studies used the sloping, high-reflectivity (due to high static stability) structure to indicate the upper air frontal zone. These studies

used either the backscattered signal power/SNR [Rottger, 1979 and Larsen and Rottger, 1985] or aspect ratio (ratio of vertical to off-vertical beam echo power) [Caccia et al., 2000; Bertin et al., 2001]. On the other hand, Vaughan and Worthington [2000] argued that a layer of enhanced horizontal wind shear may better represents the fold. Although the aforementioned studies have utilized a particular property and the radar parameter corresponding to it to identify the fold, in reality, all the above properties are imperative and should be used collectively to identify the fold, as described below.

The fold is identified, if the radar shows,

1. A sharp change in the altitude of the tropopause. In general, the magnitude of the change varies from 1 to 2 km.
2. A sloping high reflectivity structure from the tropopause into the middle/lower troposphere.
3. Wind velocities of more than 30 ms^{-1} (WMO definition of the jet stream) in the upper troposphere (between the sloping structure and the tropopause, in particular).
4. Large wind shears along the frontal zone, as a result of strong horizontal temperature gradients.

Note that a fully automated algorithm has not been developed for identifying the frontal zone, such as in Lucas et al. [2001]. Continuous measurements as a function of height and time are warranted to develop such algorithms. Low power VHF radars, such as ESRAD, although they generally provide observations from near surface (1 km) to the tropopause level continuously, suffer at times from very weak backscattered echo strength for the signals coming from the upper troposphere. These signals will not yield reliable data products. Even in such circumstances, ESRAD obtains strong backscatter

from the tropopause region (because of the aspect sensitivity) and therefore the data can be used to identify the tropopause. The present analysis (deriving fold statistics from 11 years of observations), therefore, involves both objective and subjective analysis. The objective analysis includes, the detection of the tropopause, following Hooper and Arvelius [2000]. The days when the tropopause variations are larger than 1 km in 3 hours are delineated from the total data base and are inspected for other conditions.

The total number of tropopause folds, detected by the above method, from 11 years of ESRAD measurements is 289 with a percentage fold occurrence of 7.4%. The percentage fold occurrence/frequency is defined as: 100*total number of folds /total number of observational days. The percentage fold occurrence obtained in the present study is larger in comparison with those based on ozonesonde measurements at European mid-latitude stations (3-5 %) [Beekmann et al., 1997]. However, the observed percentage occurrence of folds at Esrange is nearly equal to that reported by Nastrom et al. [1989]. Note that, Nastrom et al. [1989] analysis is also based on VHF radar measurements. They used 11 months of Flatland radar measurements for their study. The number of tropopause folds in each month as a function of month is shown in figure 7. Also included in the figure is the percentage fold occurrence for each month illustrating the annual variation of folds. A significant variation is seen in the annual cycle of the tropopause folds over Esrange with large number of folds in winter (December-February) (109 with ~11% occurrence) and fewer in summer (June-August) (36 with 4% occurrence). In particular, the number of folds is large in February and small in August with a maximum to minimum amplitude of 3.72.

However, it is possible that these statistics may have some biases, for instance, large number of folds in one month in a particular year can increase the frequency of folds in that month. To ensure that the statistics are free from such biases, the number of folds in each year is plotted as a function of month (Figure 8). The annual cycle in most years is similar to that seen for the total number of folds (Figure 7) with larger number of folds in winter and fewer in summer. Though there exists a large interannual variation of folds, no statistically significant trends are apparent nor any anomalous years (except April 2007) which could bias the statistics in Figure 7. The interannual variability is found to be larger (smaller) in Jan-Apr (May-Aug and Dec) than in other seasons. Among winter periods, larger number of folds is observed in 1996-97 (17) followed by 2002-03, 1997-98, 1999-00. The winter maximum in 1996-97 is larger than in 2000-01 by a factor greater than 2. It is interesting to note significant increase in number of folds in spring 2007 compared to other years. Inspection of surface and upper-air weather charts and detailed PV analysis corroborated the passage of large number of frontal systems over the radar location.

4. Discussion:

According to the original concept, proposed by Bjerknes and Palmen [1937] and Reed and Danielsen [1959], the tropopause fold is the region with multiple stable layers near the tropopause. These stable layers appear in temperature soundings at different altitudes, although they represent the same folded discontinuity. Since then our understanding of tropopause folds has advanced to a great extent with the availability of high resolution measurements, refined models and better concepts to represent these

features (for example, PV). Although the basic concept remained the same, subsequent studies used different (both dynamical and chemical) signatures of the fold for identifying it in different data sets.

Tropopause folds are associated with strong baroclinicity and upper level frontogenesis and typically result in deep intrusions of stratospheric air into the middle and even the lower troposphere. The intruded stratospheric air, with high ozone mixing ratio and PV, and low relative humidity, is quite different from the background tropospheric air, which is characterized by low ozone and PV and high humidy. This contrast can be used to identify the tropopause fold. Van Haver et al. [1996] and Beekmann et al. [1997] identified the folds using an automatic fold detection algorithm by assigning threshold values to the tracers of stratospheric intrusions (ozone, relative humidity and static stability). Although the air in the fold always satisfies the above conditions, but the reverse is not necessarily true. In other words, a layer of originally stratospheric ozone does not necessarily indicate the simultaneous presence of a tropopause fold. There are other STE processes (for example the breakup of stratospheric filaments) which can transport the stratospheric air into the troposphere and the transported air can satisfy the conditions used by Van Haver et al. [1996], Beekmann et al. [1997].

The techniques based on dynamical tracers (like PV, Q-vector divergence), from meteorological analysis, to identify the tropopause fold may also fail at times. For instance, many of the earlier studies depend on the topology of a threshold PV surface (for example, 2 PVU) to identify the folded structure. However, diabatic (latent and

radiative heating/cooling) and frictional processes can modify PV even in the absence of stratospheric intrusion [Bithell et al., 1999]. Though with additional criterion (such as specific humidity) it is possible to discriminate the tropopause folds unambiguously [Sprenger et al., 2003], the validity of highly variable meteorological parameters, such as humidity, (in both space and time) in analysis data sets may be questionable.

The percentage of failures in detecting folds unambiguously with the above methods (based on PV, RH and O_3) is difficult to quantify. Nevertheless, the present observations clearly indicate that the VHF radar is another promising tool for unambiguous detection of upper air frontal zones. The added advantage of utilizing VHF profilers for such studies is that the evolution of the fold can be studied with a much better resolution (as good as 1 minute in time and 150/300 m in height, as shown in case studies) than any other instruments and techniques. Further, VHF radars readily provide turbulence information (see figures 2d and 5d), which is very crucial for estimating the ozone flux across fold boundaries [Rao and Kirkwood, 2005].

Although radar detection of tropopause folds looks simple and straightforward, several problems complicate the identification process. On many occasions, a change in the tropopause altitude has been noticed. These tropopause undulations are thought to be caused by upward propagating atmospheric waves generated in the troposphere, such as mountain waves and gravity waves. Note that Esrange is on the leeward side of the Scandinavian ridge with respect to the westerly jet. The change in the tropopause altitude in these cases is more gradual than the sharp change seen in the tropopause fold cases. Layers of enhanced reflectivity are often seen in the height-time-intensity plots from ESRAD. These stable layer structures have been observed, particularly in the upper

troposphere, for more than two decades with VHF radars and are thought to arise from thin temperature sheets [Luce et al., 2001]. These stable layers have been studied in light of their, so-called, aspect sensitivity, which is significant for radars operating at VHF band. Indeed, the property of the aspect sensitivity by VHF radars has been effectively utilized by many researchers to detect frontal zones in the radar data [Caccia and Cammas, 1998; Campistron et al., 1999; Caccia et al., 2000 and Bertin et al., 2001]. On many occasions (non-folding cases), persistent stable layer structures are seen in the form of horizontal layers without significant slope. Although on some occasions these structures have been modulated by atmospheric waves, their slopes have still been found to be small in comparison with what is typically seen for a tropopause fold. In contrast to the stable layer structures, short-lived enhanced reflective structures are also seen in the vicinity of the jet stream. These layers could be turbulent layers as they coincide well with regions of large wind shears. The turbulent layers are seen for a short duration and can be distinguished from the frontal zone. However, the other dramatic consequence of jet stream dynamics is the generation of inertio-gravity (IG) waves. Utilizing radar data, Thomas et al. [1999] found a source for IG wave in the jet stream. The energy propagation by these waves was found to be upward in the stratosphere and downward in the troposphere with vertical wavelengths of 1.7 to 2.3 km [Thomas et al., 1999]. These waves can modulate the tropopause and sloping structures. Their short vertical wavelengths could lead to modulation of tropopause height similar to the 1-2 km tropopause change criteria used for the detection of a fold. However, IG waves and tropopause folds are concomitant as they are both associated to jet stream dynamics (not necessarily always). Several studies have shown that upper air frontal zones (tropopause

folds) are prolific producers of IGW [Thomas et al., 1999]. The filamentary lamina structures seen in tropopause folds are, in fact, linked to vertically differentiable advection by IGW [Danielsen et al. 1991]. Further, the turbulence generated in the wave saturation processes is an effective mechanism for exchange of air between the stratosphere and the troposphere [Bertin et al., 2001]. Although, variations associated with IG waves and stable horizontal layers could satisfy some of the conditions used for the tropopause fold detection, they would fail to satisfy other conditions. It is thus reasonable to assume that the tropopause fold alone can satisfies all the conditions outlined above and the fold statistics presented here are reliable.

5. Summary and Conclusions:

Continuous measurements by ESRAD over 11 years have been utilized to build a climatology of tropopause folds over an Arctic station, Esrange. Two distinct case studies have been studied in detail, with the help of synoptic maps of wind fields and potential vorticity, and vertical profiles of wind and humidity of radiosoundings near to the radar site. The general characteristics of the radar measurements during tropopause folding are identified from the case studies presented here and also from several tropopause folding events available in the literature. Based on these characteristics a method has been devised to identify the fold and we have shown that this method is as good as other tropopause fold detection methods. The number of folds identified by the above method from 11 years of radar observations is 289.

The present climatology of folds at around 67º N shows a significant seasonal cycle with a maximum in winter and minimum in summer. This climatology is consistent

with those reported by Ebel et al. [1996] and Elbern et al. [1998] using PV maxima and upper tropospheric Q-vector divergence as indicators. It is also consistent with Sprenger et al's [2003] identification of tropopause folds as areas with multiple crossings of the dynamical tropopause (2 PVU) in pseudosoundings using global analysis data. Note that the statistics of the above global climatologies are based on the averaged folds, where the average is taken either over a hemisphere or over a latitudinal belt. Interestingly, the present fold statistics differ from the statistics reported at midlatitudes by Van Haver et al. [1996] and Blonsky and Speth [1998]. The latter used ozonesonde measurements to identify the folds. Beekmann et al. [1997] compared three existing fold detection algorithms [by Van Haver et al., 1996; Blonsky and Speth, 1998 and Ebel et al., 1996/Elbern et al., 1998] and found that the Ebel et al. [1996]/Elbern et al. [1998] (i.e, PV/Q-vector maxima) algorithm detected all the folds seen by the other two algorithms. However, the reverse is not true. Blonsky and Speth's [1998] algorithm, which employs more stringent conditions compared to other algorithms, detects only more pronounced folds and may miss borderline cases [Beekmann et al. 1997]. This could be one reason for the smaller % occurrence of folds at mid-latitudes compared to our results.

If we assume that medium-deep/direct stratospheric intrusions are associated with tropopause folds, as they mostly do, as evidenced from various case studies in our observations and also in the literature, the winter maximum in fold frequency is consistent with the results obtained by Elbern et al. [1997], James et al. [2003], Sprenger and Wernli [2003] and Stohl [2001] using dynamical tracers. Further, studies using chemical/radionuclide tracers (such as ^{7}Be), humidity and O_3 at mountain peak stations have also shown a winter maximum and a summer minimum in the seasonal cycle of

direct stratospheric intrusions [Elbern et al., 1997; Cristofanelli et al., 2006 and references therein). This is plausible as these deep intrusions, generally associated with baroclinic eddies within storm tracks, have both geographical and seasonal preference [Seo and Bowman, 2001, Stohl et al., 2003a, Sprenger and Wernli, 2003, Stohl et al., 2003b], for instance, predominating in winter in the extratropics.

Given the fact that aforementioned studies were carried out not only with different techniques but also either at selected locations or on hemispherical scale, it is difficult to ascribe the differences in the fold climatology to a particular factor. Indeed, it is difficult to determine how much variability of fold frequency is associated with geographical variability and how much is due to the assumptions implicit in fold identification techniques. For instance, cut-off lows, favorable regions for tropopause folds, show geographical and seasonal (for example, summer over central Europe) preference [Price and Vaughan, 1992]. They, perhaps, increase the number of folds in summer at central European stations, which may result into a weak annual cycle of folds. In such a case, the differences in fold climatology seen at Esrange and at central European stations are real and represent the spatial variability of fold frequency.

Though the present climatology agrees with some of the hemispherically/ latitudinally averaged fold climatologies, it differs from others. This indicates the need to build fold climatologies at important geographical locations; and synthesize them in order for a better comparison with the global climatologies. Further, the present climatology may form a basis for fold detecting techniques based on model, reanalysis and satellite data sets to check their performance.

Acknowledgments:

The authors would like to thank Norwegian Institute for Air Research (Norsk Institutt for Luftforskning, NILU), European Centre for Medium-Range Weather Forecasting (ECMWF), and Swedish Space Corporation, Esrange for providing data used for this study. This work is carried out under a collaboration project between NARL and IRF, funded by Swedish Research Council, Sweden (No. 348-2006-5850). One of the authors (TN) is thankful to Department of Space, India for their support in formulating this collaborative project.

References:

Ancellet, G., M. Beekmann, and A. Papayannis (1994), Impact of a cutoff low development on downward transport of ozone in the troposphere, *J. Geophys. Res.*, *99*, 3451-3468.

Appenzeller, C., and H.C. Davies (1992), Structure of stratospheric intrusions into the troposphere, *Nature*, *358*, 570.

Appenzeller, C., H.C. Davies, and W.A. Norton (1996), Fragmentation of stratospheric intrusions, *J. Geophys. Res.*, *101*, 1435-1456.

Beekmann, M., et al. (1997), Regional and global tropopause fold occurrence and related ozone flux across the tropopause, *J. Atmos. Chem.*, *28*, 29-44.

Bertin, F., B. Campistron, J.L. Caccia, and R. Wilson (2001), Mixing processes in a tropopause folding observed by a network of ST radar and lidar, *Ann. Geophys.*, *19*, 953-963.

1 Bithell, M., L. J. Gray, and B. D. Cox (1999), A three-dimensional view of the evolution
2 of midlatitude stratospheric intrusions, *J. Atmos. Sci*., *56*, 673-688.
3 Bjerknes, J., and E. Palmen (1937), Investigations of selected European cyclones by
4 means of serial ascents, *Geophys. Publ.*, *12*, 1–62.
5 Blonsky, S., and P. Speth (1998), An algorithm to detect tropopause folds from ozone
6 soundings, *Meteorol Zeitschrift*, *N.F. 7*, 153-162.
7 Browell, E.V., E.F. Danielsen, S. Ismail., G.L. Gregory, and S.M. Beck (1987),
8 Tropopause fold structure determined from airborne lidar and in situ measurements,
9 *J. Geophys. Res.*, *92*, 2112-2120.
10 Caccia, J.L., and J. P. Cammas (1998), VHF-ST radar observations of an upper-level
11 front using vertical and oblique-beam C_n^2 measurements, *Mon. Wea. Rev.*, *126*, 483-
12 501.
13 Caccia J.L., F. Bertin, B. Campistron, V. Klaus, Y. Pointin, J. van Baelen, and R. Wilson
14 (2000), Cut-off low monitoring by the French VHF-ST-radar network during the
15 ESTIME campaign, *J. Atmos. Solar. Terr. Phys.*, *62*, 639-651.
16 Campistron, B., Y.B. Pointin, F. Lohou, and J.P. Pages (1999), Aspect sensitivity of VHF
17 radar echoes observed in the middle and upper troposphere during the passage of a
18 cut-off low, *Radio Sci.*, *34*, 667-779.
19 Chilson, P.B., S. Kirkwood, and A. Nilsson (1999), The Esrange MST radar: A brief
20 introduction and procedure for range validation using balloons, *Radio Sci.*, *34*, 427-
21 436.
22 Cristofanelli, P., P. Bonasoni, L. Tositti, U. Bonafe`, F. Calzolari, F. Evangelisti,

S. Sandrini, and A. Stohl (2006), A 6-year analysis of stratospheric intrusions and their influence on ozone at Mt. Cimone (2165 m above sea level), *J. Geophys. Res.*, *111*, D03306, doi:10.1029/2005JD006553.

Danielsen, E. F. (1968), Stratospheric-tropospheric exchange based on radioactivity, ozone and potential vorticity, *J. Atmos. Sci.*, *25*, 502-528.

Danielsen, E., R. S. Hipskind, W. Starr, J. Vedder, S. Gaines, D. Kley, and K. Kelly (1991), Irreversible transport in the stratosphere by internal waves of short vertical wavelengths, *J. Geophys. Res*., *96*, 17 433–17 452.

Ebel, A., H. Hass, H. J. Jakobs, M. Laube, M. Memmesheimer, A. Oberreuter, H. Geiss, and Y.H. Kuo (1991), Simulation of ozone intrusion caused by a tropopause fold and cut-off low, *Atmos Environ.*, *25A*, 2131-2144.

Ebel, A., H. Elbern, J. Hendricks, and R. Meyer (1996), Stratosphere-troposphere exchange and its impact on the structure of the lower stratosphere, *J. Geomag. Geoelectr.*, *48*, 135-144.

Elbern, H., J. Kowol, R. Sladkovic, and A. Ebel (1997), Deep stratospheric intrusions: A statistical assessment with model guided analyses, *Atmos. Environ*., *31*, 3207– 3226.

Elbern, H., J. Hendricks, and A. Ebel (1998), A climatology of tropopause folds by global analysis, *Theor. Appl. Climatol.*, *59*, 181-200.

Fuenzalida, H. A., R. Sanchez, and R. Garreaud (2005), A climatology of cutoff lows in the Souterhn hemisphere, *J. Geophys. Res*., *110*, D18101, doi:10.1029/2005JD005934.

Gage, K.S., and J. L. Green (1979), Tropopause detection by partial specular reflection with very-high-frequency radar, *Science*, *203*, 1238-1240.

1 Holton, J. R., P. Haynes, M. McIntyre, A. Douglass, R. Rood, and L. Pfister (1995),
2 Stratosphere-troposphere exchange, *Rev. Geophys*., *33*, 403-439.
3 Hooper, D. A., and J. Arvelius (2000), Monitoring of the Arctic winter tropopause: A
4 comparison of radiosonde, ozonesonde and MST radar observations, *Proc. of MST9-*
5 *COST76*, Toulouse, France, March 13-18.
6 Hooper, D. A., J. Arvelius, and K. Stebel (2004), Retrieval of atmospheric static stability
7 from MST radar return signal power, *Ann. Geophys., 22*, 3781-3788.
8 Hoskins, B.J., and F.P. Bretherton (1972), Atmospheric frontogenesis models:
9 mathematical formulation and solution, *J. Atmos. Sci.*, *29*, 11-37.
10 James, P., A. Stohl, C. Forster, S. Eckhardt, P. Seibert, and A. Frank (2003), A 15-year
11 climatology of stratosphere – troposphere exchange with a Lagrangian particle
12 dispersion model, part B, Mean climate and seasonal variability, *J. Geophys. Res.*,
13 *108(D12)*, doi:10.1029/2002JD002639.
14 Kentarchos, A. S., and T. D. Davies (1998), A climatology of cutoff lows at 200 hPa in
15 the Northern Hemisphere, 1990-1994, *Int. J. Climatol.*, *18*, 379-390.
16 Keyser, D., and M.A. Shapiro (1980), A review of the structure and dynamics of upper-
17 level frontal zones, *Mon. Weather Rev.*, *114*, 452-499.
18 Kiladis, G. N. (1998), Observations of Rossby waves linked to convection over the
19 eastern tropical Pacific, *J. Atmos. Sci*., *55*, 321– 339.
20 Lamarque, J.F., and P. Hess (1994), Cross-tropopause mass exchange and potential
21 vorticity budget in a simulated tropopause folding, *J. Atmos. Sci.*, *51*, 2246-2269.
22 Larsen, M.F., and J. Rottger (1985), Observations of frontal zone and tropopause
23 structures with a VHF Doppler radar and radiosondes, *Radio Sci.*, *20*, 1223-1232.

1 Lucas, C., P. T. May, and R. A. Vincent (2001), An algorithm for the detection of fronts
2 in wind profiler data, *Weather Forecasting*, *16*, 234–247.
3 Luce, H., M. Crochet, and F.Falaudier (2001), Temperature sheets and aspect sensitive
4 radar echoes, *Ann. Geophys.*, *19*, 899-920.
5 Luce, H., G. Hassenpflug, M. Yamamoto, and S. Fukao (2007), Comparisons of
6 refractive index gradient and stability profiles measured by balloons and the MU
7 radar at a high vertical resolution in the lower stratosphere, *Ann. Geophys.*, *25*, 47-57.
8 Martius, O., C. Schwierz, and H. C. Davies (2007), Breaking waves at the tropopause in
9 the wintertime Northern hemisphere: Climatological analyses of the orientation and
10 the theoretical $LC_{1/2}$ Classification, *J. Atmos. Sci., 64*, 2576-2593.
11 Nastrom, G.D., J.L. Green, M.R. Peterson,and K.S. Gage (1989), Tropopause folding and
12 the variability of the tropopause height as seen by the Flatland VHF radar, *J. Appl.*
13 *Meteorol.*, *28*, 1271-1281.
14 Nieto, R., et al. (2007), Climatological features of cutoff low systems in the Northern
15 hemisphere, *J. Climate, 18*, 3085-3103.
16 Ottersten, H. (1969), Mean vertical gradient of potential refractive index in turbulent
17 mixing and radar detection of CAT, *Radio Sci.*, *4*, 1247-1249.
18 Price, J.D., and G. Vaughan (1992), Statistical studies of cutoff low systems, *Ann.*
19 *Geophys.*, *10*, 96-102.
20 Price, J.D., and G. Vaughan (1993), The potential for stratosphere-troposphere exchange
21 in cutoff low systems, *Quart. J. Roy. Meteorol. Soc.*, *119*, 343-365.
22 Rao, T. N., and S. Kirkwood (2005), Characteristics of tropopause folds over Arctic
23 latitudes, *J. Geophys. Res.*, *110*, D18102, doi:10.1029/2004JD005374.

Rao, T. N., S. Kirkwood, J. Arvelius, P. von der Gathen, and R. Kivi (2003), Climatology of UTLS ozone and the ratio of ozone and potential vorticity over northern Europe, *J. Geophys. Res.*, *108*(*D22*), doi:10.1029/2003JD003860.

Reed, R. J., and E. F. Danielsen (1959), Fronts in the vicinity of the tropopause, *Arch. Meteorol. Geophys. Bioklimatol.*, *A11*, 1 – 17.

Reid, S. J., and G. Vaughan, Lamination in ozone profiles in the lower stratosphere (1991), *Q. J. R. Meteorol. Soc*., *117*, 825– 844.

Rottger, J. (1979), VHF radar observations of a frontal passage, *J. Appl. Meteorol.*, *18*, 85-91.

Seo, K.-H., and K. P. Bowman (2001), A climatology of isentropic cross-tropopause exchange, *J. Geophys. Res*., *106*, 28,159– 28,172.

Shapiro, M. A. (1980), Turbulent mixing within tropopause folds as a mechanism for the exchange of chemical constituents between the stratosphere and the troposphere, *J. Atmos. Sci.*, *37*, 994-1004.

Sprenger, M., and H. Wernli (2003), A northern hemispheric climatology of cross-tropopause exchange for the ERA15 time period (1979-1993), *J. Geophys. Res.*, *108*(*D12*), doi:10.1029/2002JD002636.

Sprenger, M., M. Croci Maspoli, and H. Wernli (2003), Tropopause folds and cross-tropopause exchange: A global investigation based upon ECMWF analysis for the time period March 2000 to February 2001, *J. Geophys. Res*., *108*(*D12*), doi:10.1029/2002JD002587.

Sprenger, M., H. Wernli and M. Bourqui (2007), Stratosphere-troposphere exchange and its relation to potential vorticity streamers and cut-offs near the extratropical tropopause, *J. Atmos. Sci.*, *64*, 1587-1602.

Stohl, A. (2001), A one-year Lagrangian ‘‘climatology’’ of airstreams in the Northern Hemisphere troposphere and lowermost stratosphere, *J. Geophys. Res.*, *106*, 7263–7279.

Stohl, A. et al. (2003a), Stratosphere-troposphere exchange: A review and what we have learned from STACCATO, *J. Geophys. Res.*, *108*(*D12*), doi:10.1029/2002JD002490.

Stohl, A., H. Wernli, P. James, M. Bourqui, C. Forster, M. A. Liniger, P. Seibert, and M. Sprenger (2003b), A new perspective on stratosphere-troposphere exchange, *Bull. Am. Meteorol. Soc.*, *84*, 1565–1573.

Thomas, L., R.M. Worthington, and A.J. McDonald (1999), Inertia-gravity waves in the troposphere and lower stratosphere associated with a jet stream exit region, *Ann. Geophys.*, *17*, 115-121.

Van Haver P., D. De Muer, M. Beekmann, and C. Mancier (1996), Climatology of tropopause folds at midlatitudes, *Geophys. Res. Lett*., *23*, 1033-1036.

Vaughan, G., and R. M. Worthington (2000), Break-up of a stratospheric streamer observed by MST radar, *Q. J. R. Meteorol. Soc*., *126*, 1751–1769.

Vaughan, G., H. Gouget, F. M. O’connor, and D. Wier (2001), Fine-scale layering on the edge of a stratospheric intrusion, *Atmos. Environ*., *35*, 2215– 2221.

Waugh, D.W. (2005), Impact of potential vorticity intrusions on subtropical upper tropospheric humidity, *J. Geophys. Res*., *110*, D11305, doi:10.1029/2004JD005664.

Wernli, H., and M. Sprenger (2007), Identification and ERA-15 climatology of potential vorticity streamers and cutoffs near the extratropical tropopause, *J. Atmos. Sci*., *64*, 1569-1586.

Wimmers, A. J., and J. L. Moody (2004), Tropopause folding at satellite observed spatial gradients: 2. Development of an empirical model, *J. Geophys. Res*., *109*, D19307, doi:10.1029/2003JD004146.

World Meteorological Organisation (WMO) (1986), Atmospheric Ozone 1985, *Global Ozone Res. And Monit. Proj., WMO Rep. 16*, Geneva.

Figure Captions:

Figure 1: Synoptic evolution of a streamer during 16–17 January 2003, (left panel) horizontal wind speed on 300 hPa surface at 12 UT on (top) 16 January 2003 and (bottom) 17 January 2003 and (right panel) potential vorticity on 310 K surface (top) at 18 and 00 UT on 16-17 January 2003 and (bottom) at 06 and 12 UT on 17 January 2003. The letters K, B, and L in the figure indicate Kiruna, Bodo, and Luleå, respectively.

Figure 2: Time-height cross sections of ESRAD parameters during the passage of tropopause fold on 17 January 2003. (a) signal-to-noise ratio (SNR), (b) zonal velocity (ms^{-1}), (c) meridional velocity (ms^{-1}), and (d) spectral width (ms^{-1})

Figure 3: Vertical profiles of wind speed, wind direction and relative humidity observed at (top) Bodo and (bottom) Luleå.

Figure 4: Same as figure 1, but for 30-31 July 2005 illustrating the synoptic evolution of a cut-off low centered north of Scandinavia

Figure 5: Same as figure 2, but for 31 July 2005

Figure 6: Same as figure 3, but for 30-31 July 2005

Figure 7: Accumulated number of folds for 11 years observed with ESRAD in each month, illustrating the annual cycle of tropopause folds at Esrange. Overlaid is the profile of % occurrence of folds as a function of month

Figure 8: Monthly variation of tropopause fold occurrence during the period, September 1996 – August 2007, illustrating the Interannual variation of tropopause folds. Overlaid is the profile of percentage occurrence of folds as a function of month

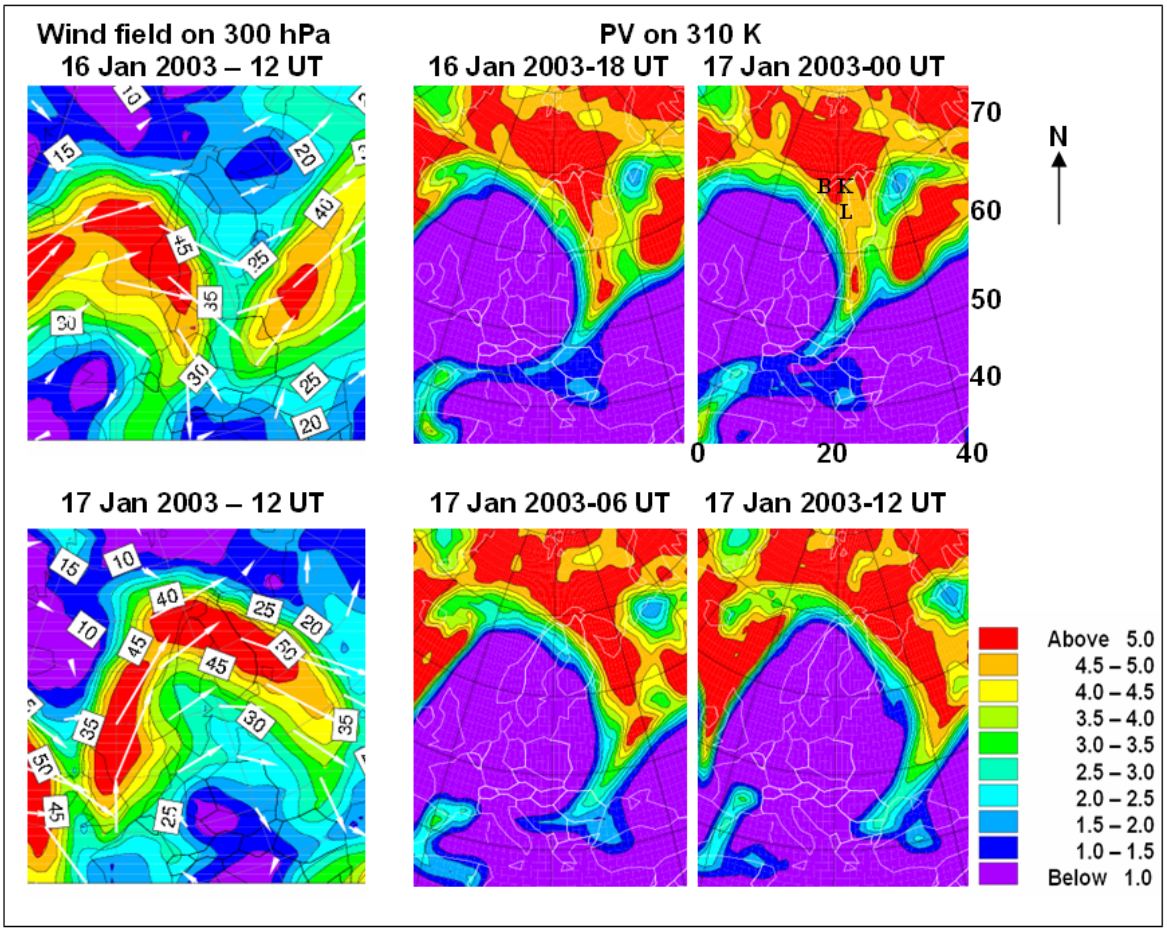

Figure 1: Synoptic evolution of a streamer during 16–17 January 2003, (left panel) horizontal wind speed on 300 hPa surface at 12 UT on (top) 16 January 2003 and (bottom) 17 January 2003 and (right panel) potential vorticity on 310 K surface (top) at 18 and 00 UT on 16-17 January 2003 and (bottom) at 06 and 12 UT on 17 January 2003. The letters K, B, and L in the figure indicate Kiruna, Bodo, and Luleå, respectively.

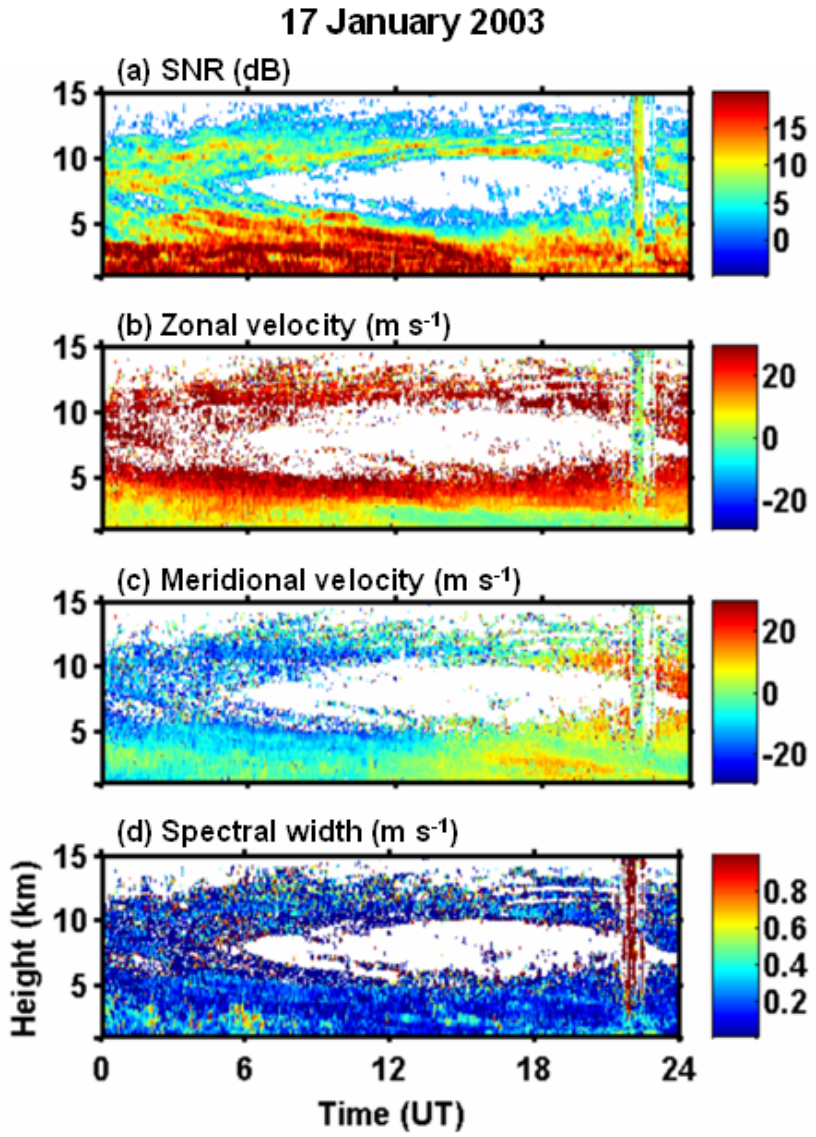

Figure 2: Time-height cross sections of ESRAD parameters during the passage of tropopause fold on 17 January 2003. (a) signal-to-noise ratio (SNR), (b) zonal velocity (ms^{-1}), (c) meridional velocity (ms^{-1}), and (d) spectral width (ms^{-1})

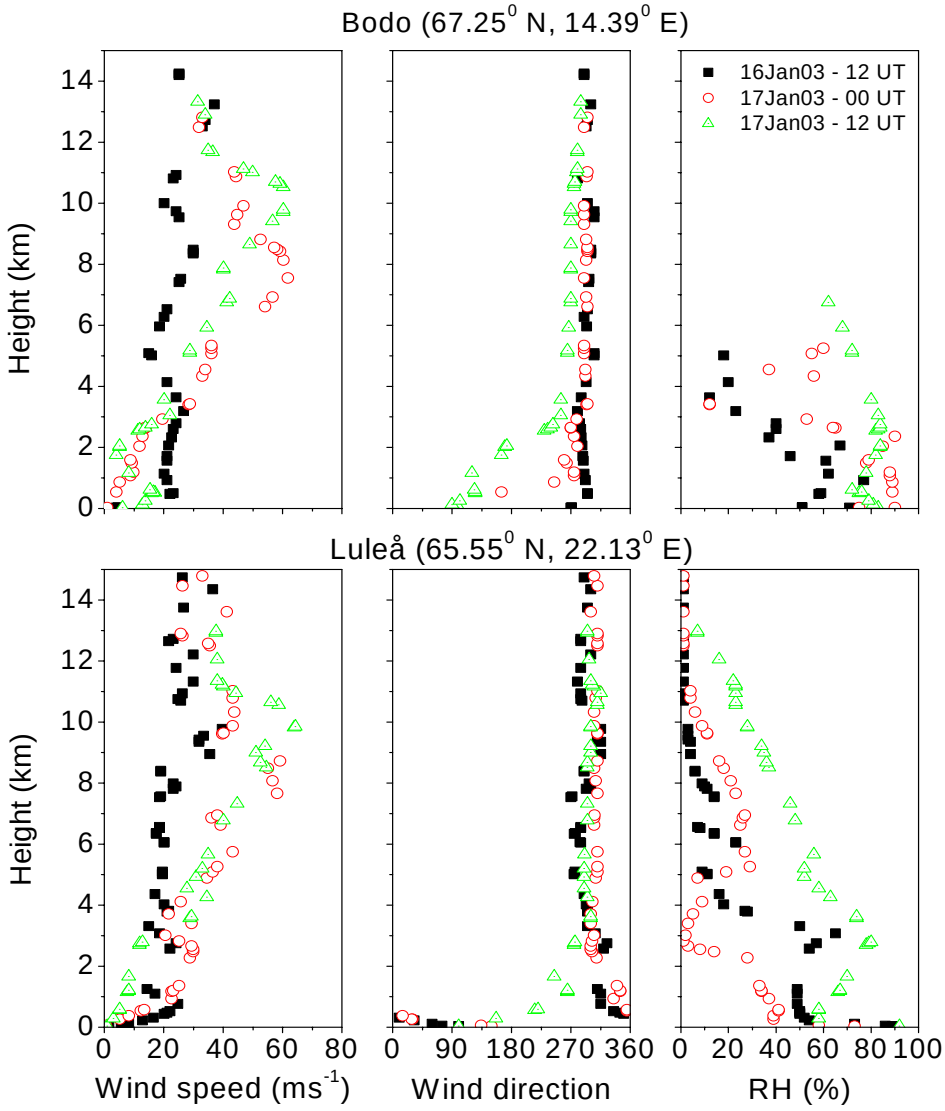

Figure 3: Vertical profiles of wind speed, wind direction and relative humidity observed at (top) Bodo and (bottom) Luleå.

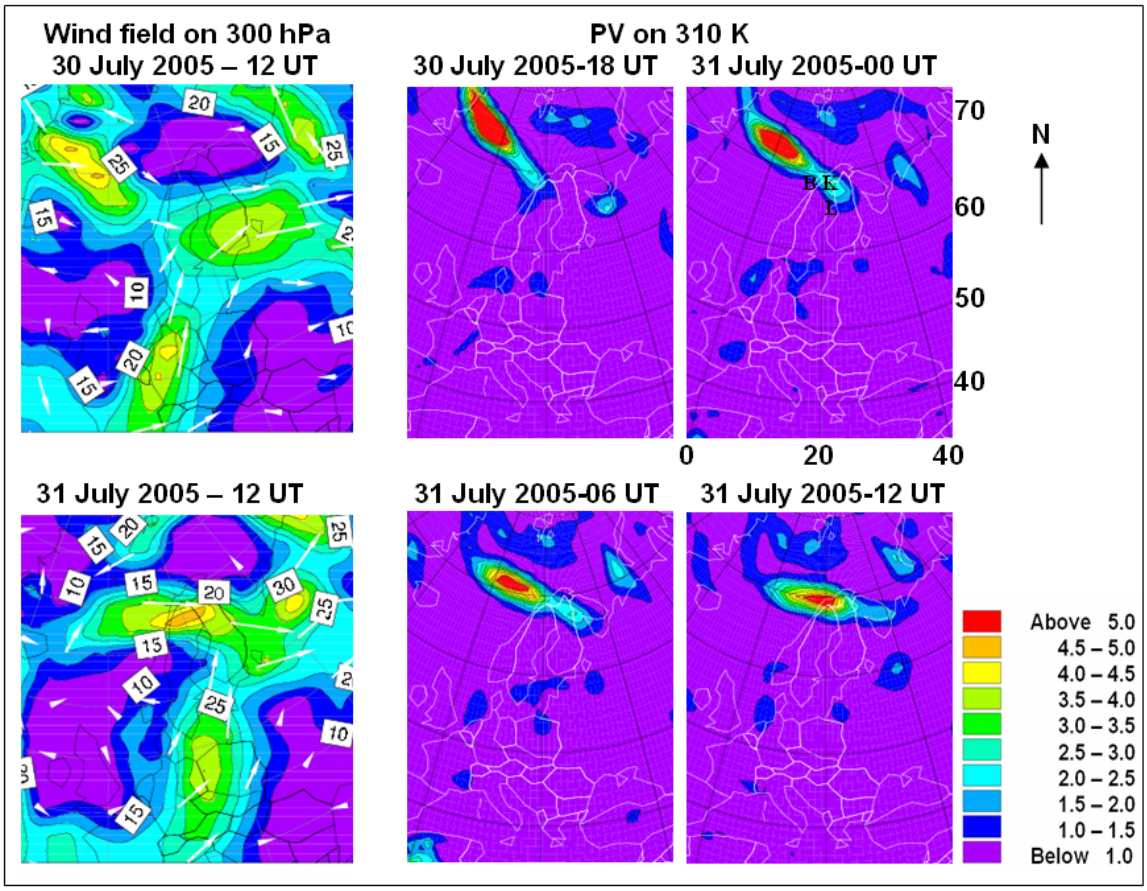

Figure 4: Same as figure 1, but for 30-31 July 2005 illustrating the synoptic evolution of a cut-off low centered north of Scandinavia

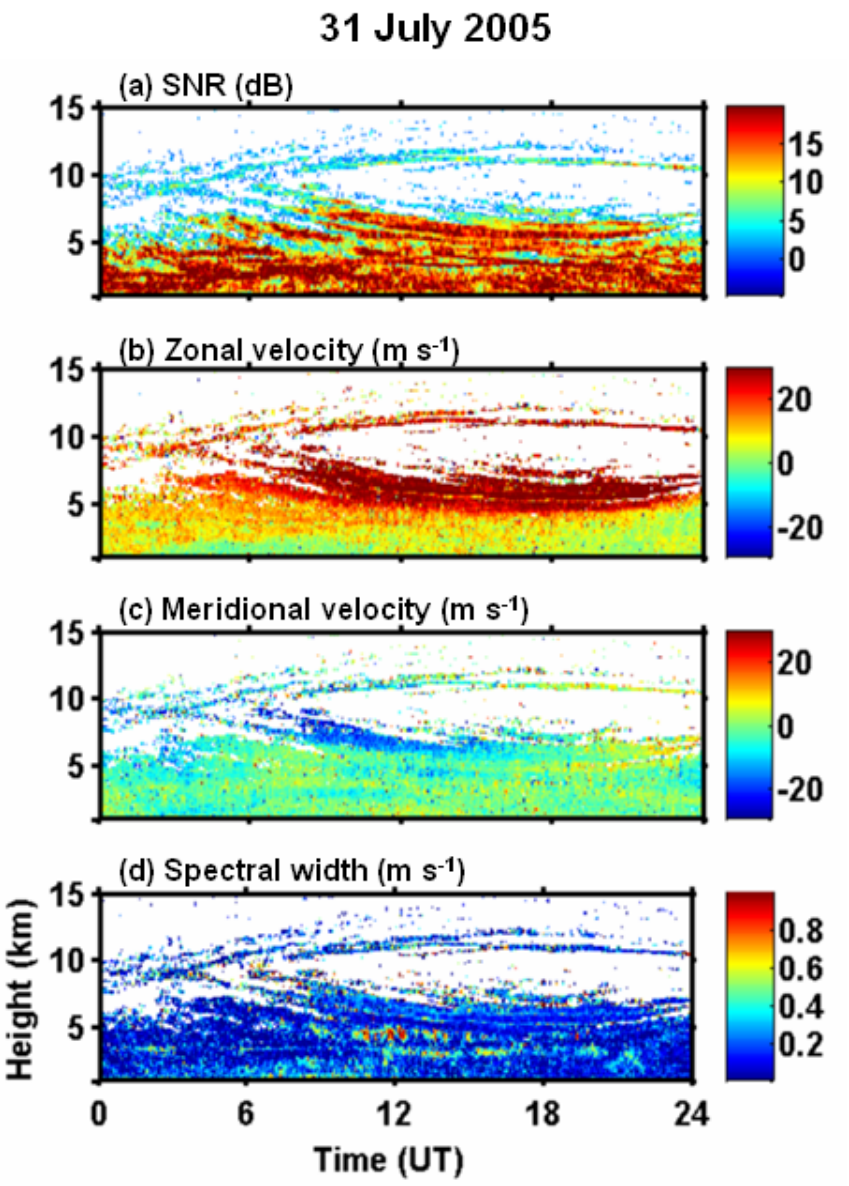

Figure 5: Same as figure 2, but for 31 July 2005

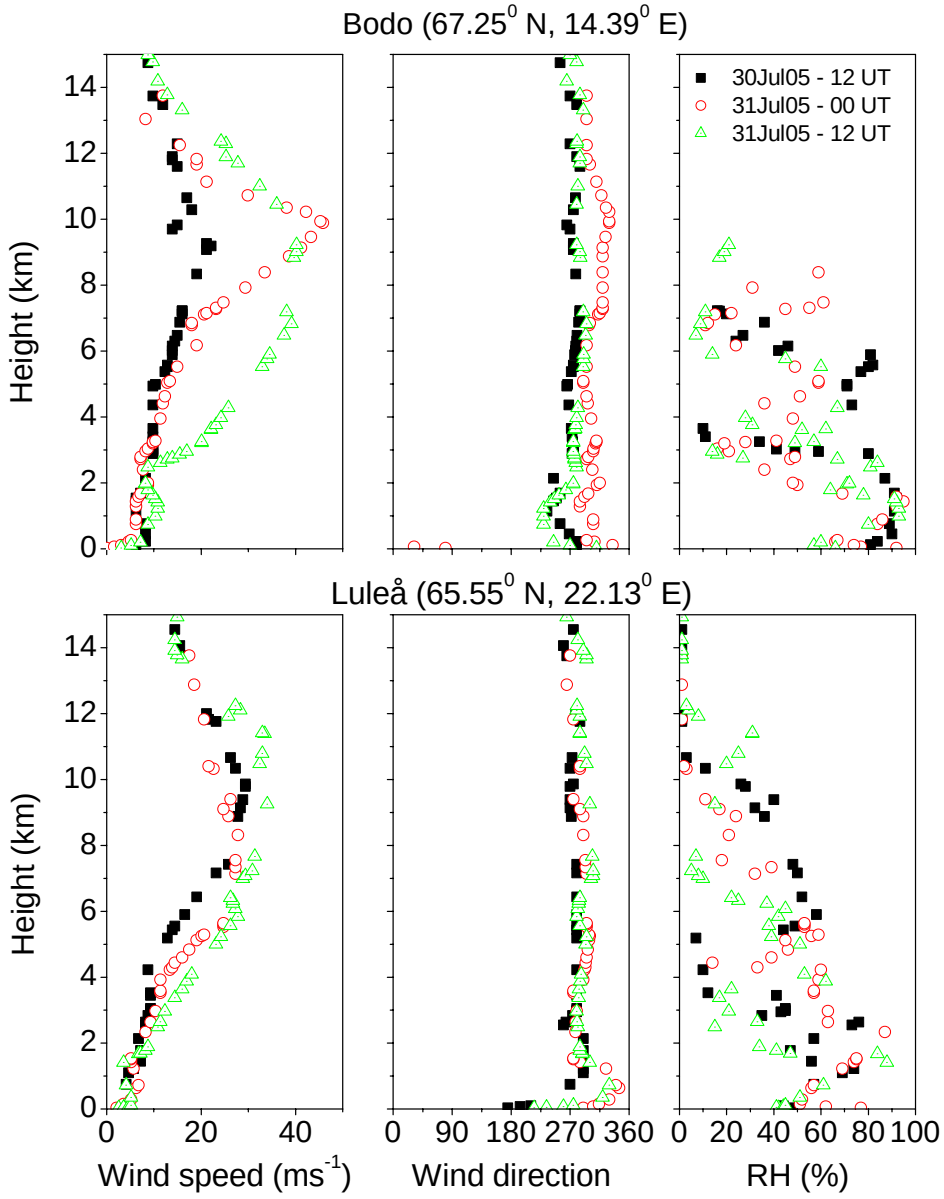

Figure 6: Same as figure 3, but for 30-31 July 2005

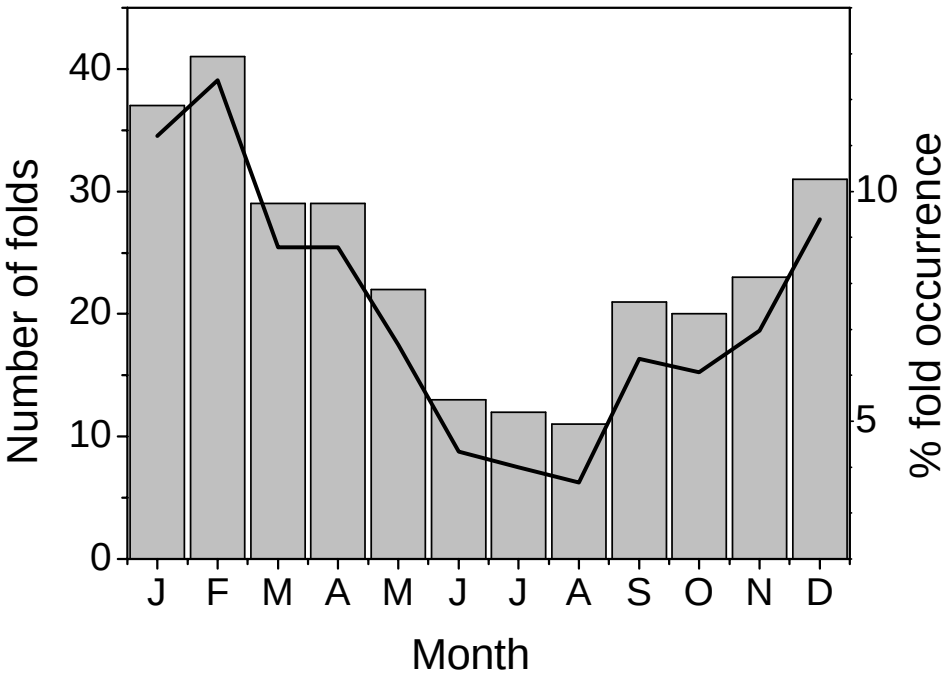

Figure 7: Accumulated number of folds for 11 years observed with ESRAD in each month, illustrating the annual cycle of tropopause folds at Esrange. Overlaid is the profile of percentage occurrence of folds as a function of month

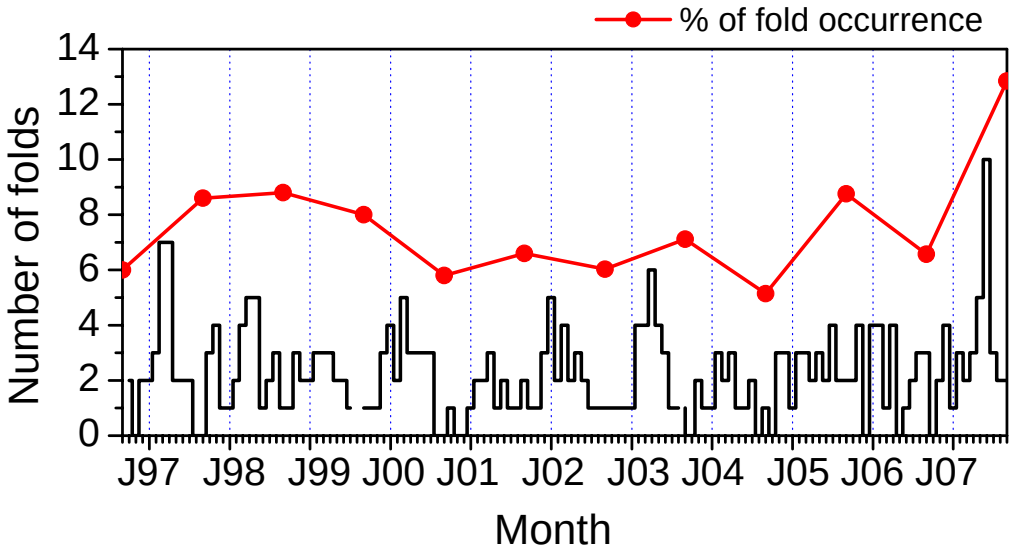

Figure 8: Monthly variation of tropopause fold occurrence during the period, September 1996 – August 2007, illustrating the Interannual variation of tropopause folds. Overlaid is the profile of percentage occurrence of folds as a function of month